Semicond. Sci. Technol. **24** (2009) 045002 (5pp) doi:10.1088/0268-1242/24/4/045002

# The silicon on dust substrate path to make solar cells directly from a gaseous feedstock

**J M Serra, C R Pinto, J A Silva, M C Brito, J Maia Alves and A M Vallêra**

SESUL/Faculdade de Ciências da Universidade de Lisboa, Campo Grande ED-C8, 1749-016 Lisboa, Portugal

E-mail: jmserra@fc.ul.pt

Received 1 October 2008, in final form 27 January 2009
Published 24 February 2009
Online at stacks.iop.org/SST/24/045002

**Abstract**

In this paper, we present a silicon on dust substrate (SDS) process, a new method for the growth of silicon ribbons. As a demonstration of the concept, we also present results on solar cells made of these new silicon ribbons. SDS ribbons were obtained directly from a gaseous feedstock by a fast CVD step using silane. The resulting self-supported intrinsic ribbons were microcrystalline and porous. To make these ribbon films suitable for photovoltaic applications, a novel recrystallization with an *in situ* doping step was developed. To this purpose, the ribbons were sprayed with boric acid and then recrystallized by float zone melting. Simple solar cells were prepared by employing: aluminium back contacts, Ti/Pd/Ag front grid contacts, with no anti-reflective coating, doping optimization, passivation or gettering. The 1-sun *I–V* characteristics of the cells were: $V_{oc} \sim 530$ mV and $J_{sc} \sim 24$ mA cm$^{-2}$. The minority carrier diffusion length obtained from a spectral response at long wavelengths gave values of $L_n \sim 70$ $\mu$m.

(Some figures in this article are in colour only in the electronic version)

## 1. Introduction

The costs of commercial solar cells are dominated by the ingot/wafering step to produce the wafers. In the 1980s, it was already realized that such a wasteful process could be avoided by the direct preparation of a silicon sheet by ribbon growth techniques. Although easy to envisage, this problem proved very difficult to solve as seen by the fact that even today most solar cell industrial production relies on energy intensive silicon crystallization in an ingot form, followed by wasteful wafering.

Processes for direct growth of silicon in the form of ribbons may be classified into three different categories as follows.

(i) Direct growth of a self-supported silicon ribbon from the melt, e.g. edge-defined film growth (EFG) [1] and string ribbon [2].
(ii) Growth on an incorporated substrate, with the substrate remaining attached to film, e.g. at FhISE, Germany [3] and IMEC, Belgium [4].
(iii) Growth on a substrate, with detachment and re-utilization of the substrate, e.g. ribbon growth on substrate (RGS) [5] and silicon sheet from powder (SSP) [6].

Previous R&D on silicon ribbon growth on substrates has focused on either non-detachable silicon films on cheap substrates or detachable films on high-quality silicon substrates.

In a silicon on dust substrate (SDS) process presented here (see the flow diagram in figure 1) a layer of silicon dust, obtained from a high purity gaseous feedstock, placed on a quartz plate, acts both as a place for deposition and as a 'sacrificial detachment layer'. Second, a thick film is deposited on the bedding layer by fast CVD, at low temperatures and atmospheric pressure. Finally, the detached free standing ribbon is sprayed with a boric acid solution and it is recrystallized by a floating molten zone (zone melting recrystallization (ZMR)) technique.

For the vapour phase deposition, silane ($SiH_4$) is an excellent feedstock because of its homogeneous nucleation and high deposition rates at low temperatures (about

 

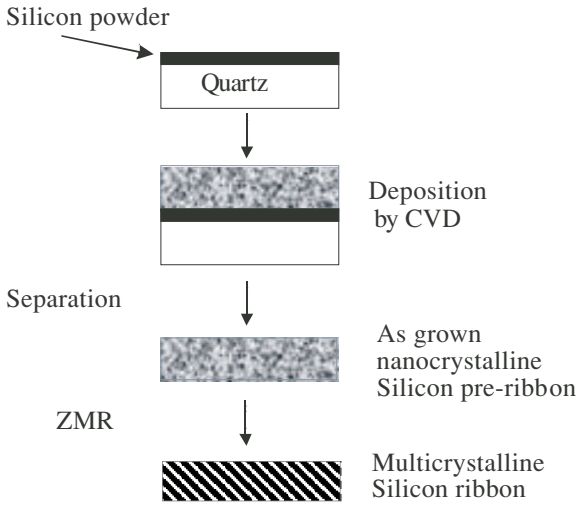


**Figure 1.** Flowchart of the SDS process.

900 °C) and atmospheric pressures. High deposition rates can be used because of the separation of the CVD deposition and crystallization steps.

The advantages of the SDS process are as follows: (i) no substrate and therefore no associated cost and no contamination, (ii) low energy and thermal budget by use of atmospheric pressures and low temperature CVD and (iii) high quality, free standing, crystalline silicon sheet by float zone crystallization, with no contact with foreign materials.

The SDS process is well suited for a continuous mode. For example, at a 20 $\mu$m min$^{-1}$ deposition rate (achievable with silane at ∼900 °C), only 10 min is required to achieve a 200 $\mu$m thick pre-ribbon. With such a deposition rate and considering a constant advance speed of 10 mm min$^{-1}$ during the recrystallization step, only a 100 mm long high temperature (900 °C) zone is required for the pre-ribbon formation.

## 2. Experimental procedure

Silicon deposition by CVD on top of a layer of silicon powder, placed over a quartz plate, is used to deposit a so-called pre-ribbon. The powder layer, which remains between the quartz plate and the deposited pre-ribbon, allows easy detachment of this pre-ribbon. By ZMR processing, this pre-ribbon is converted into a multicrystalline ribbon that can be used as the base for solar cells.

### *2.1. Pre-ribbon formation*

A powder layer with an area of 12 cm$^2$, 0.5 mm in thickness, with a density between 0.23 and 0.29 g cm$^{-3}$ is placed on top of a quartz plate inside the CVD reactor. CVD deposition occurs on top of this layer of silicon powder.

A specially designed furnace is used to grow the silicon pre-ribbons. In the work we present here, a batch configuration of the CVD deposition furnace was employed instead of a continuous mode furnace. The only difference is that the quartz substrate with the silicon powder does not move inside the furnace. This furnace has a top window through which radiation from halogen lamps is used to heat a layer of silicon powder placed on top of a quartz plate sample holder. The heated silicon powder triggers the silane decomposition and acts as a seed for the deposition of silicon. Conditions that are normally avoided in CVD processes are employed (powder formation, and fast, low crystalline quality growth) because the aim is to attain high growth rates rather than crystal quality (table 1).

**Table 1.** CVD parameters used in this study.

| Temp. (°C) | Gas | Flow (l min$^{-1}$) | Dep. rate ($\mu$m min$^{-1}$) |
|---|---|---|---|
| 750–800[a] | Silane (10% in $H_2$) | 0.4 | 6–8 |

[a] The temperature in this furnace setup is limited to 800 °C.

The pre-ribbons obtained in this step are structurally unsuitable for solar cells despite their nanocrystalline structure, because of their high porosity. Several pre-ribbons were prepared, with average sheet densities between 42 and 84 mg cm$^{-2}$, corresponding to solid silicon thicknesses between 180 and 360 $\mu$m, with varying degrees of porosity (ranging from 70% to 20%) and homogeneity.

### *2.2. Ribbon doping and recrystallization*

The pre-ribbons obtained in the CVD step are intrinsic silicon. Doping is achieved by a recently developed technique [7], where boric acid is sprayed (12 mM in deionized milli-Q water) over the pre-ribbon surface prior to the recrystallization step.

The doping process begins with the cleaning of the pre-ribbon with polish (HF + $HNO_3$ + $CH_3COOH$) and HF solutions. Then, the pre-ribbon is sprayed with a solution of boric acid with a concentration of 0.76 g l$^{-1}$. The spraying of the boric acid is carried out by using an airbrush Badger 250 fed with a fixed pressure of nitrogen in order to guarantee a reproducible and homogeneous deposition. The airbrush is located 80 cm above the sample. A 22 cm diameter cylindrical enclosure is used to prevent perturbations due to air currents.

The ZMR step is performed using an in-house-developed furnace composed of two elliptical mirrors that concentrate the radiation of two 1000 W halogen lamps [8]. The free standing pre-ribbons are held in a vertical position without the need of any substrate. This allows us to melt the pre-ribbon from both sides simultaneously and across all the ribbon thickness. The molten zone is 2.5 cm in length, 3 mm in width and the scan speed is 10 mm min$^{-1}$. During ZMR, as the temperature increases, the boric acid decomposes into boron oxide and water, which will evaporate from the surface of the sample. For temperatures above 1100 °C, boron is incorporated into the sample by diffusion across the surface forming silicon oxide (which will migrate to the surface of the sample) according to the reaction:

$$2B_2O_3(g) + 3Si(s) \rightarrow 3SiO_2(s) + 4B(s) \quad (1)$$

Above 1200 °C, however, most of the boric oxide has evaporated from the surface of the sample therefore removing the boron source for the diffusion process. The argon–boron

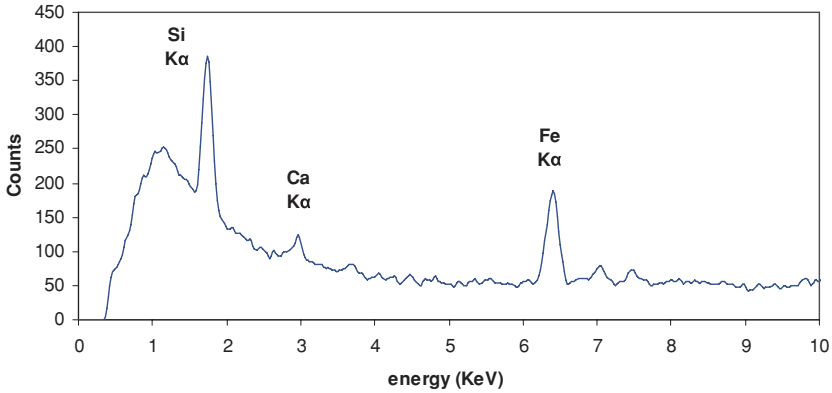


**Figure 2.** XPS spectrum of the silicon powder.

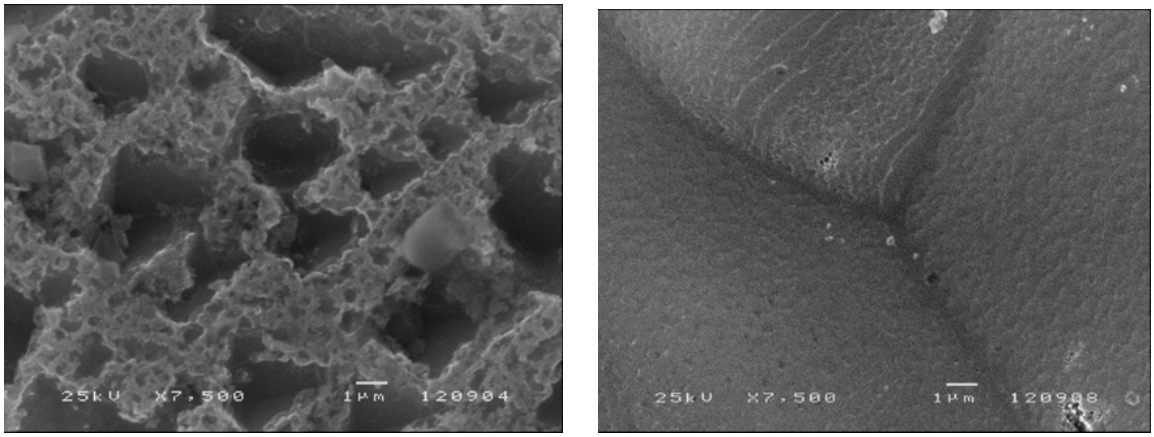


**Figure 3.** SEM picture of the pre-ribbon surface before (left) and after (right) the ZMR step.

atmosphere will then be responsible for further doping of the silicon with boron. The incorporation rate of boron into silicon during this phase is critically dependent on the argon flux, the direction of recrystallization (upwards or downwards) and its velocity (slower recrystallization leads to larger boron incorporation) [7]. In the molten zone, the boron will be uniformly mixed due to convection in the liquid. After recrystallization, the sample is cleaned with an HF solution that removes the layer of silicon oxide from the surface.

With this technique the doping and recrystallization stages were successfully combined into a single step allowing for high crystal quality whilst keeping contamination low, because the pre-ribbon does not come into contact with any foreign materials.

We point out that p- or n-doped pre-ribbons can be readily obtained by mixing appropriate gases, such as phosphine, during the CVD deposition.

Finally, it should be mentioned that the doping and ZMR steps are also suitable for continuous mode processing.

## 3. Results

### *3.1. Powder characterization*

The silicon powder bed used on top of the quartz holder is made of very fine powder grains of silicon. Although the silicon powder itself comes from the decomposition of silane gas, we found some traces of iron and calcium were observed by x-ray XPS analysis. The spectrum is shown in figure 2, revealing a high concentration of iron and traces of calcium.

### *3.2. Ribbon growth*

Diluted silane (10% in $H_2$) enters the reactor decomposing upon reaching the heated powder layer. Gas convection, gas diffusion and decomposition in the powder bed and its temperature distribution are critical parameters in controlling the pre-ribbon shape and uniformity.

It was observed that by adjusting the gas path within the furnace and the lamp power, conversion rates of silane into silicon of 60–75% could be obtained.

The porous nature of the pre-ribbon is clearly shown in figure 3. Reproducible ZMR crystallization was obtained for pre-ribbon porosities below ∼50% provided that the pre-ribbon thickness is constant.

In fact it was observed that, depending on the experimental conditions, the spatial variation of the deposition rate may yield different pre-ribbon cross section shapes: plane–convex, plane–concave or plane–plane. These different cross sections lead to different behaviour during the ZMR as shown in figure 4.

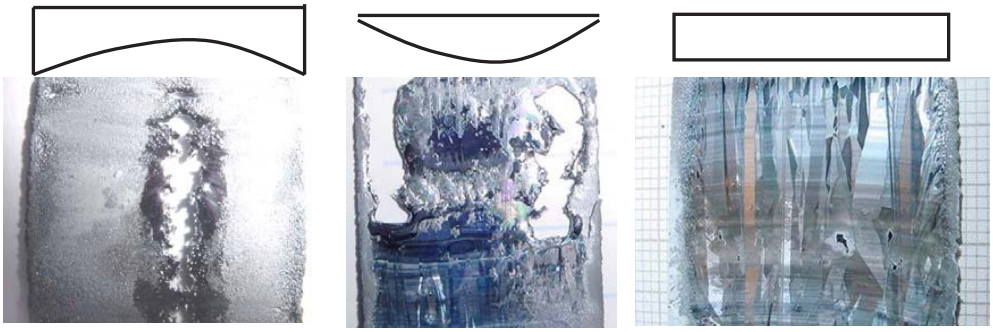

**Figure 4.** ZMR success depends on the shape of the cross section (shown above each photo) of the pre-ribbon. The ribbon width is 3 cm in all cases.

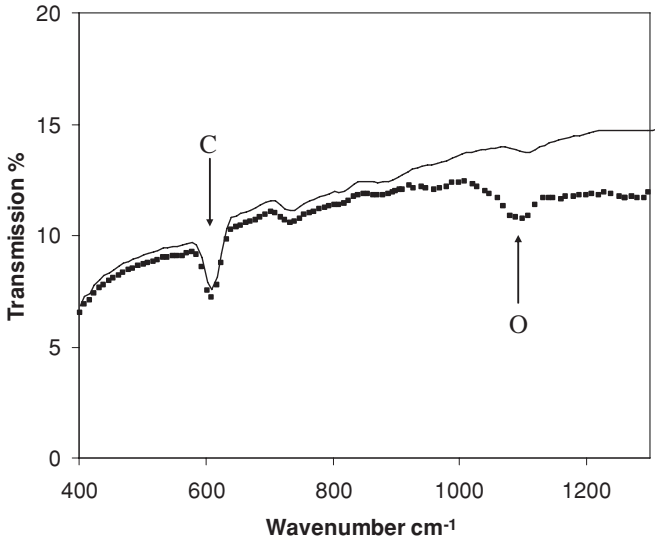


**Figure 5.** IR transmission spectrum of a typical SDS ribbon (thin line) and of a control sample—a ribbon containing interstitial oxygen (heavy dots).

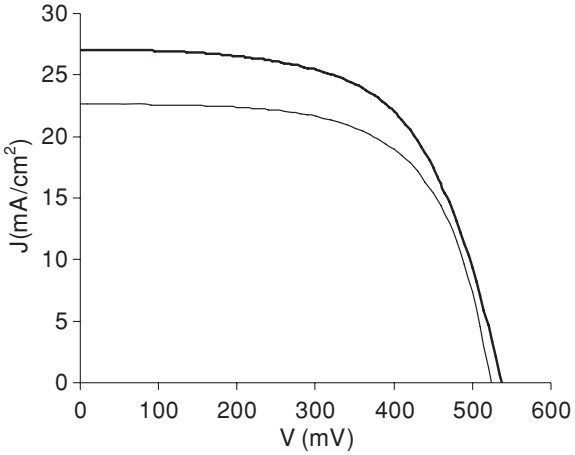


**Figure 6.** *I–V* curves of the best SDS cell and of a control cell (in bold).

**Table 2.** Solar cell typical parameters of the SDS and control samples.

| | $J_{sc}$ (mA cm$^{-2}$) | $V_{oc}$ (mV) | FF (%) | Eff. (%) |
|---|---|---|---|---|
| Control | 27.02 | 540 | 67.2 | 8.5 |
| SDS | 22.6 | 530 | 63.1 | 7.6 |

The plane–concave shape leads to holes in the middle while the plane–convex shape leads to ZMR disruption at the edges of the ribbon. The third shape, plane–plane, allowed for successful ZMR.

The recrystallized ribbons produced in this study were 300 $\mu$m thick, with a crystalline structure consisting of grains of a few centimetres long and a few millimetres wide, p-doped, with resistivities of about 1.5 Ω cm.

We also analysed these ribbons by infrared spectroscopy in order to find additional possible impurities. The IR transmission spectrum of a typical SDS ribbon (figure 5) shows the presence of substitutional carbon, indicated by the absorption band at 600 cm$^{-1}$ [9], but no interstitial oxygen since there is no measurable absorption at 1109 cm$^{-1}$ [10] as shown against a control sample which contains interstitial oxygen. The reason to investigate the presence of oxygen is related to the fact that the silicon powder used had been in contact with air, causing the formation of a layer of native silicon oxide on the surface of the powder grains. The IR data thus show that oxygen is removed during the ZMR step. Since neither the CVD deposition or the ZMR furnaces use carbon at all, one may conclude that it must be already present in the original powder used.

### *3.3. Solar cell preparation and characterization*

To evaluate the suitability of these ribbons for photovoltaic applications, solar cells were prepared aiming at the characterization of the material rather than the solar cell performance. The junction was formed by phosphorus diffusion from a solid source. After mesa etching, a grid of Ti/Pd/Ag front contacts and aluminium back contacts were deposited by vacuum thermal evaporation, followed by contact annealing. No further optimizations were included in the cell preparation, i.e. anti-reflective coatings, doping optimization, defect passivation or gettering. Some cells, made of multicrystalline cast silicon that underwent the same ZMR process, were used as control samples to test if the ZMR limited the final electronic properties of the ribbons. The solar

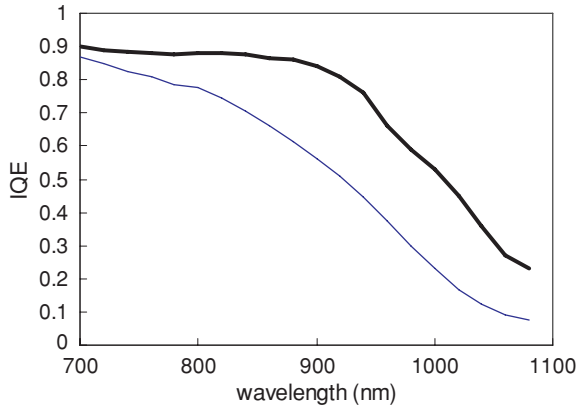


**Figure 7.** Internal quantum efficiency for the best SDS cell and the control cell (in bold).

cells were characterized by the spectral response and *I–V* curve measurements.

Figure 6 shows typical *I–V* measurements of both groups. Some more data are shown in table 2. The best SDS cell in this set of samples has $V_{oc} \sim 535$ mV and $J_{sc} = 22.6$ mA cm$^{-2}$.

The low fill factors and low $V_{oc}$ on the control cells indicate a possible problem in our cell process. Nevertheless, the data demonstrate the ability to produce solar cells directly from a gaseous feedstock.

Spectral response measurements were also made on several cells to evaluate material quality. A typical response in these cells in the long wave range (700–1100 nm) is shown in figure 7. The minority carrier diffusion length can be extracted by plotting the inverse internal quantum efficiency (IQE) versus the absorption length and computing the intercept at the horizontal axis [11], yielding a diffusion length of around 70 $\mu$m. We used optical absorption data from [12].

The short circuit current is higher in the control cells than in the SDS cells, as expected from the full spectrum quantum efficiency curves of the cells in this comparison. The relatively low $V_{oc}$ obtained in both the SDS and control cells is difficult to explain, even considering the absence of passivation. But as we have already mentioned, this is probably related to a problem during cell processing which we are trying to identify.

The quantum efficiency curves in the SDS cells are lower than those obtained for the control cells in the infrared region, indicating a smaller minority carrier diffusion length in the SDS material (see figure 7). This is in good agreement with the minority carrier diffusion length results from the spectral response at long wavelengths, which gave values of $L_n \sim 70$ $\mu$m in the SDS cells, to be compared with values of about 300 $\mu$m obtained in the control samples. Given the fact that the recrystallization process was identical for SDS and control cells, the lower diffusion length of SDS ribbon cells is probably a consequence of the impurities present in the pre-ribbon powder, namely carbon and especially iron, which is known to degrade the lifetime significantly [13]. A study on the impurities present in the silicon powder is an issue currently being addressed.

## 4. Conclusions

The silicon on dust substrate (SDS) method for the formation of silicon ribbons based on a gaseous feedstock was described, and its feasibility demonstrated by the preparation of full working photovoltaic cells on an SDS ribbon silicon. The advantages of the SDS process are as follows: (i) no substrate is required, thus reducing sources of impurity and cost; (ii) low energy budget because CVD is performed under atmospheric pressures and at low temperatures; (iii) high quality, free standing, crystalline silicon sheets are made possible by non-contact float zone crystallization with *in situ* doping.

## Acknowledgments

This work has been partially supported by the following FCT grants: SFRH/BD/10408/2002, SFRH/BD/12763/2003 and SFRH/BPD/20660/2004. We thank C Coelho for the XPS measurements.

## References

[1] Wald F 1981 *Crystals: Growth, Properties and Applications* vol 5 (New York: Springer) p 147
[2] Ciszek T 1987 *Silicon Processing for Photovoltaics I, Materials Processing Theory and Practices* vol 6 (North-Holland: Amsterdam) p 131
[3] Reber S, Eyer A, Haas F, Schillinger N, Janz S and Schmich E 2004 *Proc. 20th European Photovoltaic Conf. (Barcelona)* p 459
[4] Poortmans J 2006 *Thin Film Solar Cells* (Weinheim: Wiley-VCH) p 1
[5] Schonecker A, Laas L, Gutjahr A, Wyers P, Reinink A and Wiersma B 2002 *Proc. 29th IEEE Photovoltaic Specialists Conf. (New Orleans)* p 316
[6] Eyer A, Schillinger N and Rauber A 1989 *Proc. 9th European Photovoltaic Solar Energy Conf. (Freiburg)* p 17
[7] Silva J A, Brito M C, Costa I, Maia Alves J, Serra J M and Vallêra A M 2007 *Sol. Energy Mater. Sol. Cells* **91** 1948–53
[8] Pinto C R, Serra J M, Brito M C, Gamboa R, Maia Alves J and Vallêra A M 2006 *Proc. 21st European Photovoltaic Solar Energy Conf. and Exhibition (Dresden)* p 1099
[9] Canham L T 1988 IR absorption due to C in silicon *Properties of Silicon* (London: INSPEC) p 316
[10] Baghdadi A, Bullis W M, Croarkin M, Li Y Z, Scace R, Series R W, Stallhofer P and Watanabe M 1989 *J. Electrochem. Soc.* **136** 2015
[11] Green M A 1987 *High Efficiency Solar Cells* (Switzerland: Trans Tech Publications) p 155
[12] Swimm R and Dumas K 1982 *J. Appl. Phys.* **53** 7502
[13] Davis J R, Rohatgi A, Hopkins R H, Blais P D, Rai-Choudhury P, McCormick J R and Mollenkopf H C 1980 *IEEE Trans. Electron Devices* **ED-27** 677